MULTI-VIEW OPTIMAL PUSHBROOM TRIANGULATION

Michela Mancini [*1], Sébastien Henry[*1] and John A. Christian[1].
[1]Guggenheim School of Aerospace Engineering, Georgia Institute of Technology, 270 Ferst Drive, Atlanta, GA, 30332.
[*]These two authors contributed equally to this work.

Abstract. *The photogrammetric reconstruction of planetary terrain from images is an essential task for many planetary science missions. This task requires the determination of the 3D location of a terrain point—usually through triangulation and subsequent bundle adjustment. When the images are captured by conventional framing cameras, there are well-known and widely-used, statistically optimal solutions. Many digital terrain maps (DTMs), however, are produced using pushbroom images (and not framing camera images). The geometry of pushbroom image formation is fundamentally different, and the familiar pinhole camera model is inapplicable. In this work, we use the linear pushbroom camera model to develop a statistically optimal solution to the triangulation of a 3D point from two or more pushbroom images.*

Introduction. Pushbroom cameras are common science instruments in planetary imaging and exploration. These cameras are scanning sensors that posses a linear array of detectors which produce a one-dimensional image at any instant in time. A 2D image is obtained by stacking together sequential 1D images captured as the camera flies over the terrain. Because of the continuous exposure of their sensor array, pushbroom cameras provide more radiometrically accurate images when compared with conventional framing cameras, which is particularly useful in poor or variable illumination conditions.[1]

A common application of pushbroom images is in the construction of digital terrain maps (DTMs). Examples of pushbroom cameras used to take pictures of planetary surfaces are the Narrow Angle Camera (NAC) onboard the Lunar Reconnaissance Orbiter (LRO),[2] the Mars Express High Resolution Stereo Camera (HRSC),[3] and the High Resolution Imaging Science Experiment (HiRISE) onboard the Mars Reconnaissance Orbiter (MRO).[4]

Pushbroom cameras differ from common framing camera in that the formation of a pushbroom image is dependent upon the dynamics of the spacecraft during image capture. An accurate model of the pushbroom projection must take this into account. The motion of the camera is responsible for the high aspect ratio of pushbroom images of planetary terrains. Due to the short time window over which typical pushbroom images are captured, it is reasonable to assume that the camera has a constant speed and constant attitude. For this reason, we decided to work with the linear pushbroom camera model developed in Ref. [5]. The corresponding projection matrix can be easily derived from the camera parameters and the spacecraft state. The linear pushbroom model also has applications in aerial imagery.[6]

Since pushbroom cameras are often used in terrain reconstruction, particular attention has been given to *triangulation* in the literature. Reference [7] develops a method for 3D reconstruction from pushbroom images and demonstrates it on SPOT images,[8] a model which was then refined by Ref. [9]. A full terrain reconstruction pipeline from pushbroom images is proposed in Ref. [10]. These works inherently require bundle adjustment to determine the optimal solution. A more recent but still iterative approach is provided in Ref. 11, where the authors propose a linear pushbroom triangulation solution which uses Rational Function Model (RFM) to characterize the projection. This model is purely mathematical (i.e., not directly related to the geometry of observation) and its coefficients are not always available in satellite image metadata.[10]

Despite the ubiquity of pushbroom cameras in space applications, the authors are unaware of a non-iterative and statistically optimal solution for triangulating a point using pushbroom images. In this work, we will use the optimal framework described in Ref. [12] to develop such an optimal solution under the linear pushbroom camera model.

The linear pushbroom camera model. Begin by defining the camera frame with the z-axis along the boresight, y-axis along the 1D sensor array, and the x-axis completing the right-handed triad (positive in the direction of the camera velocity). At each instant in time, the camera position and the y-axis define the so-called *view plane*, where the one-dimensional instantaneous field of view lies. Any point in the field of view will project along the y-direction following perspective projection.[5,13] If we let $\boldsymbol{\ell}$ be the position vector of the point relative to the camera, expressed in the instantaneous camera frame, and d_y, v_p be the usual camera calibration parameters,[14] we may express the v-pixel coordinate of the point along the y-axis using

$$\begin{bmatrix} vw \\ w \end{bmatrix} = \begin{bmatrix} 0 & d_y & v_p \\ 0 & 0 & 1 \end{bmatrix} \boldsymbol{\ell} \tag{1}$$

where the parameter w was introduced to explicitly account for the scaling.

As the camera moves, the view plane sweeps out a region of space, resulting in an orthographic projection along the x-axis. A point that does not lie in the view plane at some time t_0, but is visible in the final 2D image, necessarily lies in the view plane of the camera at some other time t. Letting $\boldsymbol{\ell}_0$ be the position vector of that point relative to the camera at t_0, and $\boldsymbol{\ell}$ be the position vector of the same point relative to the camera at t, we can find the u-pixel coordinates by determining the time

at which $\ell_x = 0$. Since the motion of the camera is linear, with constant velocity $\boldsymbol{v} = [V_x\, V_y\, V_z]^T$, we have

$$\boldsymbol{\ell}_0 = \boldsymbol{\ell} + \boldsymbol{v}(t - t_0) \tag{2}$$

which yields, setting $\ell_x = 0$

$$\Delta t = t - t_0 = \frac{\ell_{0x}}{V_x} \tag{3}$$

The u-pixel coordinates may now be determined introducing the exposure time τ[5, 13]

$$u = \Delta t/\tau \tag{4}$$

The combination of Eq. (4) and Eq. (1), together with the relation in Eq. (2), provides the linear pushbroom projection projection model

$$\begin{bmatrix} u \\ vw \\ w \end{bmatrix} = \begin{bmatrix} 1/\tau & 0 & 0 \\ 0 & d_y & v_p \\ 0 & 0 & 1 \end{bmatrix} \begin{bmatrix} 1/V_x & 0 & 0 \\ -V_y/V_x & 1 & 0 \\ -V_z/V_x & 0 & 1 \end{bmatrix} \boldsymbol{\ell}_0 \tag{5}$$

recalling that $\boldsymbol{\ell}_0$ is the position vector of any point in the world relative to the camera location at time t_0.

The projection model may be easily modified to express world points in any other chosen world frame. Let $\boldsymbol{r}_0$ be the position of the camera at time t_0, expressed in the new world frame, and let $\boldsymbol{T}_C^W$ be the attitude rotation matrix from the world frame to the camera frame. Given a point $\boldsymbol{p}_W \in \mathbb{R}^3$, we may obtain $\boldsymbol{\ell}_0$ as

$$\boldsymbol{\ell}_0 = \begin{bmatrix} \boldsymbol{T}_C^W & -\boldsymbol{T}_C^W \boldsymbol{r}_0 \end{bmatrix} \begin{bmatrix} \boldsymbol{p}_W \\ 1 \end{bmatrix} = \boldsymbol{\Pi}_C^W \begin{bmatrix} \boldsymbol{p}_W \\ 1 \end{bmatrix} \tag{6}$$

and combine it with Eq. (5) to obtain the final projection model

$$\begin{bmatrix} u \\ vw \\ w \end{bmatrix} = \boldsymbol{K}\boldsymbol{B}\boldsymbol{\Pi}_C^W \begin{bmatrix} \boldsymbol{p}_W \\ 1 \end{bmatrix} \tag{7}$$

where we used

$$\boldsymbol{K} = \begin{bmatrix} 1/\tau & 0 & 0 \\ 0 & d_y & v_p \\ 0 & 0 & 1 \end{bmatrix} \tag{8}$$

$$\boldsymbol{B} = \begin{bmatrix} 1/V_x & 0 & 0 \\ -V_y/V_x & 1 & 0 \\ -V_z/V_x & 0 & 1 \end{bmatrix} \tag{9}$$

A multi-view linear solution. Assume we have $N \geq 2$ cameras that observe the same point $\boldsymbol{p}_W$ in their respective pushbroom images. A simple manipulation of the linear pushbroom model of Eq. (7) already allows us to triangulate the 3D position of that point.

Assume that the pushbroom camera i takes the picture of the point $\boldsymbol{p}_W$, and let $\boldsymbol{K}_i$, $\boldsymbol{B}_i$, $\boldsymbol{\Pi}_{Ci}^W$ be the matrices defining the corresponding projection model. The first step requires that we find an explicit expression for the scale factor w_i. This quantity is nothing more than the

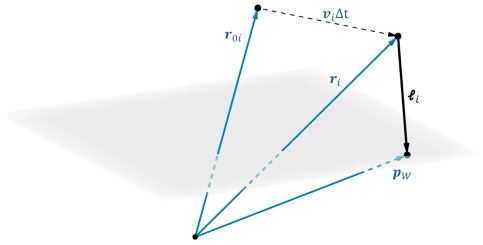

Figure 1. Relationship between the camera initial position $\mathbf{r}_{0i}$***, the camera position*** $\mathbf{r}_i$ ***at the time of the projection of the point*** $\mathbf{p}_W$ ***and the line of sight*** $\boldsymbol{\ell}_i$

z-component of the vector joining the point on the terrain and the camera at the time of the point projection, expressed in the camera frame. Recalling that this vector is $\boldsymbol{\ell}_i$, we may write (see Fig. 1)

$$w_i = \hat{\boldsymbol{z}}_i^T \boldsymbol{\ell}_{Wi} = \hat{\boldsymbol{z}}_i^T (\boldsymbol{p}_W - \boldsymbol{r}_i) \tag{10}$$

where $\hat{\boldsymbol{z}}_i$ is the direction of the z-axis of the camera frame expressed in the world frame (i.e. the third row of the matrix $\boldsymbol{T}_{Ci}^W$). Since the camera has constant velocity, we may also write

$$w_i = \hat{\boldsymbol{z}}_i^T (\boldsymbol{p}_{Wi} - \boldsymbol{r}_{0i} - \Delta t_i \boldsymbol{v}_{Wi}) \tag{11}$$

where $\boldsymbol{v}_{Wi} = \boldsymbol{T}_{Wi}^C \boldsymbol{v}$ and Δt_i comes from Eq. (4).

Substituting this result into the left-hand side of Eq. (7) and manipulating, we obtain

$$\begin{bmatrix} u_i \\ v_i w_i \\ w_i \end{bmatrix} = \begin{bmatrix} u_i \\ 0 \\ 0 \end{bmatrix} + \begin{bmatrix} 0 \\ (\boldsymbol{p}_{Wi} - \boldsymbol{r}_{0i} - \boldsymbol{v}_{Wi} u_i \tau_i)^T \hat{\boldsymbol{z}}_i v_i \\ (\boldsymbol{p}_{Wi} - \boldsymbol{r}_{0i} - \boldsymbol{v}_{Wi} u_i \tau_i)^T \hat{\boldsymbol{z}}_i \end{bmatrix} \tag{12}$$

that is

$$\begin{bmatrix} u_i \\ v_i w_i \\ w_i \end{bmatrix} = \begin{bmatrix} u_i \\ -v_i u_i \tau_i \boldsymbol{v}_{Wi}^T \hat{\boldsymbol{z}}_i \\ -u_i \tau_i \boldsymbol{v}_{Wi}^T \hat{\boldsymbol{z}}_i \end{bmatrix} + \begin{bmatrix} 0 \\ \hat{\boldsymbol{z}}_i^T v_i \\ \hat{\boldsymbol{z}}_i^T \end{bmatrix} \boldsymbol{p}_{Wi} - \begin{bmatrix} 0 \\ \hat{\boldsymbol{z}}_i v_i \\ \hat{\boldsymbol{z}}_i \end{bmatrix} \boldsymbol{r}_{0i} \tag{13}$$

The right-hand side of Eq. (7) is

$$\boldsymbol{K}_i \boldsymbol{B}_i \boldsymbol{\Pi}_{Ci}^W \begin{bmatrix} \boldsymbol{p}_w \\ 1 \end{bmatrix} = \boldsymbol{K}_i \boldsymbol{B}_i \boldsymbol{T}_{Ci}^W \boldsymbol{p}_W - \boldsymbol{K}_i \boldsymbol{B}_i \boldsymbol{T}_{Ci}^W \boldsymbol{r}_{0i} \tag{14}$$

Combining these two equations

$$\begin{aligned} \left(\boldsymbol{K}_i \boldsymbol{B}_i \boldsymbol{T}_{Ci}^W - \begin{bmatrix} 0 \\ v_i \hat{\boldsymbol{z}}_i^T \\ \hat{\boldsymbol{z}}_i^T \end{bmatrix} \right) \boldsymbol{p}_W = \\ \begin{bmatrix} u_i \\ -v_i u_i \tau_i \boldsymbol{v}_{Wi}^T \hat{\boldsymbol{z}}_i \\ -u_i \tau_i \boldsymbol{v}_{Wi}^T \hat{\boldsymbol{z}}_i \end{bmatrix} - \left(\begin{bmatrix} 0 \\ v_i \hat{\boldsymbol{z}}_i^T \\ \hat{\boldsymbol{z}}_i^T \end{bmatrix} - \boldsymbol{K}_i \boldsymbol{B}_i \boldsymbol{T}_{Ci}^W \right) \boldsymbol{r}_0 \end{aligned} \tag{15}$$

which is a linear system of the form

$$\boldsymbol{A}_i \boldsymbol{p}_W = \boldsymbol{b}_i \tag{16}$$

Because of scale ambiguity, the matrix $\boldsymbol{A}_i$ is not full rank and at least two pushbroom images are necessary to sufficiently determine the system. We can formulate the system to solve as

$$\boldsymbol{A}\boldsymbol{p}_W = \boldsymbol{b}, \tag{17}$$

where $\boldsymbol{A}$ and $\boldsymbol{b}$ are defined as

$$\boldsymbol{A}^T = \begin{bmatrix}\boldsymbol{A}_1^T & \dots & \boldsymbol{A}_N^T\end{bmatrix},\ \boldsymbol{b}^T = \begin{bmatrix}\boldsymbol{b}_1^T & \dots & \boldsymbol{b}_N^T\end{bmatrix},\ N \geq 2 \tag{18}$$

The solution of this least-square problem may be found with classical approaches.

Optimal triangulation. The least-squares solution obtained solving the system of equations of Eq. (17) is not optimal in a statistical sense. This section highlights a way to obtain the maximum likelihood estimate (MLE) from the previously obtained equations. The derivation follows a similar approach to regular the multi-view optimal triangulation in Ref.[12].

First, note that Eq.16 only holds in the case where the measurements constituting the system are perfect. However, the measurements come from noisy sources in real applications. There is thus a residual term which can be written as

$$\boldsymbol{\epsilon}_i = A_i\boldsymbol{p}_W - \boldsymbol{b}_i. \tag{19}$$

The residual $\boldsymbol{\epsilon}_i \neq 0$ in real applications due to error sources such as landmark localization errors. Let us then assume that the measured landmark pixel locations deviate from their true locations with a Normal distribution, $\tilde{u} = u + \mathcal{N}(0, \sigma_u)$ and $\tilde{v} = v + \mathcal{N}(0, \sigma_v)$. Assuming these errors to be uncorrelated, we can propagate this uncertainty to compute the covariance of $\boldsymbol{\epsilon}_i$ as

$$\boldsymbol{R}_{\boldsymbol{\epsilon}_i} = \sigma_u^2 \boldsymbol{J}_{u_i}\boldsymbol{J}_{u_i}^T + \sigma_v^2 \boldsymbol{J}_{v_i}\boldsymbol{J}_{v_i}^T \tag{20}$$

where the partials are

$$\boldsymbol{J}_{u_i} = \frac{\partial \boldsymbol{\epsilon}_i}{\partial u_i} = \begin{bmatrix} -1 \\ v_i\tau_i \boldsymbol{v}_{Wi}^T \boldsymbol{z}_i \\ \tau_i \boldsymbol{v}_{Wi}^T \boldsymbol{z}_i \end{bmatrix} \tag{21}$$

$$\boldsymbol{J}_{v_i} = \frac{\partial \boldsymbol{\epsilon}_i}{\partial v_i} = \begin{bmatrix} 0 \\ (\boldsymbol{p}_W - \boldsymbol{r}_0 + \Delta t_i \boldsymbol{v}_{Wi})^T \boldsymbol{z}_i \\ 0 \end{bmatrix} \tag{22}$$

The reader will note that the covariance $\boldsymbol{R}_{\boldsymbol{\epsilon}_i}$ cannot be full rank due to the fact that $\boldsymbol{\epsilon}_i$ is the residual of an underconstrained equation. However, the eigenvector of $\boldsymbol{R}_{\boldsymbol{\epsilon}_i}$ corresponding to the 0 eigenvalue is naturally orthogonal to the residual vector $\boldsymbol{\epsilon}_i$. It then is possible to use the pseudo-inverse to formulate the MLE cost-function

$$J(\boldsymbol{p}_W) = \sum_i \boldsymbol{\epsilon}_i^T \boldsymbol{R}_{\boldsymbol{\epsilon}_i}^\dagger \boldsymbol{\epsilon}_i. \tag{23}$$

To minimize the cost function in Eq. 24, take its derivative with respect to $\boldsymbol{p}_W$ and set it to zero, so

$$J(\boldsymbol{p}_W) = \sum_i (\boldsymbol{A}_i\boldsymbol{p}_W - \boldsymbol{b}_i)^T \boldsymbol{R}_{\boldsymbol{\epsilon}_i}^\dagger (\boldsymbol{A}_i\boldsymbol{p}_W - \boldsymbol{b}_i), \tag{24}$$

$$\left(\sum_i \boldsymbol{A}_i^T \boldsymbol{R}_{\boldsymbol{\epsilon}_i}^\dagger \boldsymbol{A}_i\right) \boldsymbol{p}_W = \left(\sum_i \boldsymbol{A}_i^T \boldsymbol{R}_{\boldsymbol{\epsilon}_i}^\dagger \boldsymbol{b}_i\right). \tag{25}$$

It is apparent that prior knowledge of $\boldsymbol{p}_W$ is necessary to obtain $\boldsymbol{R}_{\boldsymbol{\epsilon}_i}$. However, $\boldsymbol{p}_W$ is unknown and is precisely the variable we seek to estimate. To remedy this, we can create a coarse initial estimate of $\boldsymbol{p}_W$, which will be the topic of the next section.

Providing an initial guess. The optimal triangulation approach presented in this section requires an initial guess of the the position vector $\boldsymbol{p}_W$, which may be obtained in at least two ways.

Both approaches require the determination of the range λ between a camera and the observed point. Given the position of the camera i at the initial time t_{0i}, we can determine its position at the time t_i of the point projection by combining Eq. (2) and Eq. (4)

$$\boldsymbol{r}_i = \boldsymbol{r}_{0i} + \boldsymbol{v}_{Wi} u_i \tau_i \tag{26}$$

Since the line of sight from the camera to the point must belong to the instantaneous view plane (where the field of view lies), the position vector of the point on the terrain may be obtained as

$$\boldsymbol{p}_W = \boldsymbol{r}_i + \lambda_i y_i \hat{\boldsymbol{y}}_i + \lambda_i \hat{\boldsymbol{z}}_i \tag{27}$$

where $\hat{\boldsymbol{y}}_i$ is the direction of the y-axis of the camera frame expressed in the world frame, λ_i is the unknown scaling factor and y_i is the image plane coordinate associated with v_i

$$y_i = (v_i - v_{Pi})/d_{yi} \tag{28}$$

If the mean radius of the orbited planet is available, then a single camera may be used, and a coarse estimate of the point $\boldsymbol{p}_W$ may be obtained by selecting the smallest λ_i such that $\|\boldsymbol{p}_{Wi}\| = R_{planet}$, as shown in Fig.2. This requires the solution of a simple quadratic system. If we let

$$a = 1 + y_i^2 \tag{29a}$$

$$b = y_i \boldsymbol{r}_i^T \hat{\boldsymbol{y}}_i + \boldsymbol{r}_i^T \hat{\boldsymbol{z}}_i \tag{29b}$$

$$c = \boldsymbol{r}_i^T \boldsymbol{r}_i - R_{planet}^2 \tag{29c}$$

then λ_i will be the smallest among

$$\lambda_{i1,i2} = \frac{-b \pm \sqrt{b^2 - ac}}{a} \tag{30}$$

Alternatively, if the orbited planet is unknown, the ranges λ_i and λ_j corresponding to two cameras i and j may be found by imposing that the right-hand side of Eq. (27) is the same for the cameras i and j. Any two equations of this system can be used to solve for the unknown ranges. For example, setting

$$\begin{bmatrix} p_{i1} \\ p_{i2} \end{bmatrix} = \begin{bmatrix} y_i\hat{y}_{i,1} + \hat{z}_{i,1} \\ y_i\hat{y}_{i,2} + \hat{z}_{i,2} \end{bmatrix} \tag{31}$$

and defining p_{j1}, p_{j2} similarly, we may determine the unknown ranges as

$$\lambda_j = \frac{p_{i,1}(r_{iy} - r_{jy}) + p_{i,2}(r_{jx} - r_{ix})}{p_{i,1}p_{j,2} - p_{i,2}p_{j,1}} \tag{32a}$$

$$\lambda_i = 1/p_{i,1}\left(r_{jx} - r_{ix} + \lambda_j p_{j,1}\right) \tag{32b}$$

Table 1. Results of a Monte Carlo simulation with $100,000$ ***runs and*** 1 ***pixel of noise in both directions on a simulated LLO case.***

	$\Delta p_{Wx}\,[km]$		$\Delta p_{Wy}\,[km]$		$\Delta p_{Wz}\,[km]$	
	bias	std. dev	bias	std. dev	bias	std. dev
linear	3.4639×10^{-5}	1.8257×10^{-2}	-3.50726×10^{-5}	1.6111×10^{-2}	-2.2034×10^{-5}	1.0015×10^{-2}
optimal	-5.5651×10^{-7}	3.0002×10^{-3}	-3.3691×10^{-6}	2.0810×10^{-3}	-2.7777×10^{-6}	2.1487×10^{-3}

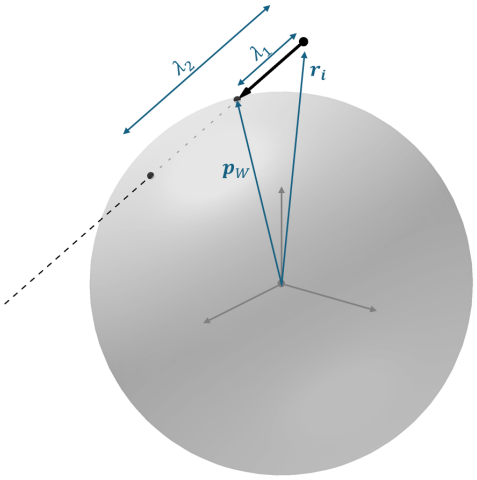

Figure 2. The line of sight from the camera intersects a spherical planet at two points, but only the point with smaller range λ_1 ***is actually visible.***

Experimental results. Consider two pushbroom cameras with the following parameters:

$$\boldsymbol{r}_{0_1} = \begin{bmatrix} -1252.8 \\ 1037.7 \\ -923.91 \end{bmatrix} \text{km},\ \boldsymbol{v}_{0_1} = \begin{bmatrix} -1.0937 \\ -1.1965 \\ 0.1233 \end{bmatrix} \text{km/s} \quad (33)$$

$$\boldsymbol{r}_{0_2} = \begin{bmatrix} -1256.5 \\ 1033.8 \\ -887.67 \end{bmatrix} \text{km},\ \boldsymbol{v}_{0_2} = \begin{bmatrix} -0.9237 \\ -1.3269 \\ -0.2397 \end{bmatrix} \text{km/s} \quad (34)$$

(35)

These two cameras take pictures of the same point in space. For a perfectly spherical Moon, this point lies at

$$\boldsymbol{p}_W = \begin{bmatrix} -1129.9 \\ 867.2 \\ -995.9 \end{bmatrix} km \quad (36)$$

In our experiments, we assumed fluctuations in the point's elevation using 3 km of standard deviation. Applying noise to the ideal pixel coordinates of the point in the two images, we can perform a Monte Carlo simulation and compare the performance of the solution provided by the linear system with the performance of the optimal solution.

In this simulation, we used the initial guess provided by Eq. (30), which requires the knowledge of the Moon's radius. Since, in reality, the Moon is not a perfect sphere, we modeled fluctuations in the lunar radius by sampling a normal distribution with zero mean and five kilometers of standard deviation. We also applied an error with zero-mean and 1 pixel of standard deviation to both the u and v pixel coordinates of the point's projection in the two pushbroom images.

Both methods are able to provide the correct solution, with the statistically optimal approach being more accurate in 91% of the cases. More details on the statistics of the simulation may be found in Table 1.

Conclusions. In this work, we presented a solution to the triangulation of a point from two or more pushbroom images which leverages the pushbroom linear projection model. The first approach proposed, while simply requiring a solution of a linear system, does not guarantee statistical optimality. The second solution presented, instead, is statistically optimal in the sense that it minimizes the reprojection error of the point in the pushbroom images. Both the solutions are non-iterative, and their performance is analyzed with a Monte Carlo simulation.

References.

[1] J. R. Jensen, *Remote Sensing of the Environment: An Earth Resource Perspective*. Prentice Hall Series in Geographic Information Science, Upper Saddle River, NJ: Pearson Prentice Hall, 2nd ed., 2007.

[2] M. S. Robinson and et al., "Lunar reconnaissance orbiter camera (LROC) instrument overview," *Space Science Reviews*, vol. 150, pp. 81–124, 1 2010.

[3] G. Neukum and R. Jaumann, "HRSC: The High Resolution Stereo Camera of Mars Express," in *Mars Express: The Scientific Payload*, vol. 1240, pp. 17–35, 2004.

[4] A. S. McEwen and et al., "Mars Reconnaissance Orbiter's High Resolution Imaging Science Experiment (HiRISE)," *Journal of Geophysical Research: Planets*, vol. 112, no. E5, 2007.

[5] R. Gupta and R. I. Hartley, "Linear pushbroom cameras," *IEEE Transactions on Pattern Analysis and Machine Intelligence*, vol. 19, no. 9, pp. 963–975, 1997.

[6] V. O. Jonassen, C. Ressl, N. Pfeifer, *et al.*, "Bundle adjustment of aerial linear pushbroom hyperspectral images with sub-pixel accuracy," *PFG – Journal of Photogrammetry, Remote Sensing and Geoinformation Science*, 2024.

[7] V. Kratky, "Rigorous photogrammetric processing of spot images at ccm canada," *ISPRS Journal of Photogrammetry and Remote Sensing*, vol. 44, no. 2, pp. 53–71, 1989.

[8] M. Chevrel, M. Courtois, and G. Weill, "The spot satellite remote sensing mission," *Photogrammetric Engineering and Remote Sensing*, vol. 47, pp. 1163–1171, aug 1981.

[9] D. Fritsch and D. Stallmann, "Rigorous photogrammetric processing of high resolution satellite imagery," vol. XXXIII, no. Part B4, pp. 313–321, 2000.

[10] Y. Wang, X. Yang, F. Xu, A. Leason, and S. Megenta, "An operational system for sensor modeling and dem generation of satellite push broom sensor images," in *XXI Congress of the International Society for Photogrammetry and Remote Sensing (ISPRS)*, (Beijing, China), ERDAS Inc, 2008.

[11] P. Liao, G. Chen, X. Zhang, K. Zhu, Y. Gong, T. Wang, X. Li, and H. Yang, "A linear pushbroom satellite image epipolar resampling method for digital surface model generation," *ISPRS Journal of Photogrammetry and Remote Sensing*, vol. 190, pp. 56–68, 2022.

[12] S. Henry and J. A. Christian, "Absolute triangulation algorithms for space exploration," *Journal of Guidance, Control, and Dynamics*, vol. 46, no. 1, pp. 21–46, 2023.

[13] M. Mancini, A. Thrasher, C. D. Vries, and J. Christian, "Crater projection in linear pushbroom camera images," 2024.

[14] J. A. Christian, "A Tutorial on Horizon-Based Optical Navigation and Attitude Determination with Space Imaging Systems," *IEEE Access*, pp. 19,819–19,853, 2021.